Risk Averse Shape Optimization

Sergio Conti*   Harald Held†   Martin Pach†   Martin Rumpf‡

Rüdiger Schultz†

March 31, 2009

Abstract

Risk-averse optimization has attracted much attention in finite-dimensional stochastic programming. In this paper, we propose a risk-averse approach in the infinite dimensional context of shape optimization. We consider elastic materials under stochastic loading. As measures of risk awareness we investigate the *expected excess* and the *excess probability*. The developed numerical algorithm is based on a regularized gradient flow acting on an implicit description of the shapes based on level sets. We incorporate topological derivatives to allow for topological changes in the shape optimization procedure. Numerical results in 2D demonstrate the impact of the risk-averse modeling on the optimal shapes and on the cost distribution over the set of scenarios.

Key Words: shape optimization in elasticity, two-stage stochastic programming, risk aversion, level set method, topological derivative.

1 Introduction

Shape optimization for elastic bodies under deterministic loading is a well-developed field, which can be seen as an instance of PDE-constrained infinite-dimensional optimization, see e.g. the books [45, 13, 2]. In this paper we investigate shape optimization problems where an elastic body $\mathcal{O} \subset \mathbb{R}^2$ is subject to stochastic volume and surface loading. The stochastic load might arise from stochastically varying load configuration in time or from uncertainty in measurements of the forces acting on the body (cf. [18, 16, 15]). Such type of uncertainty is a prevailing issue in many real-world shape-optimization problems, in which unlikely but dramatic failures must be appropriately taken into account. Ignoring this stochasticity might lead to optimal structures that are quite vulnerable with respect to variations of loadings. This instability is clearly not a failure of the optimization procedure, but rather a modelling issue: The model should already incorporate uncertain loadings. There have been several approaches to this problematic, one of them being the *robust optimization* approach. For an overview about robust optimization we refer to [12]. This has been applied to shape optimization problems e.g. in [26, 18, 16, 15].

For each realization of the stochastic loading one evaluates a cost functional depending on the elastic domain and the elastic displacement field. Decisions on the shape have to be made before the stochastic forcing is applied. The requirement that the first-stage decision must not depend on the future observation is referred to as nonanticipativity. Obviously, optimizing the shape for a single loading pattern corresponding to the expectation value of the stochastic loading does not properly reflect this nonanticipativity requirement. Rather, one observes a striking similarity with two-stage stochastic programming, which we will elaborate on in sections 2 and 4 below. In a first attempt one might ask for shapes which minimize the expected value of the cost functional.

---

*Institut für Angewandte Mathematik, Rheinische Friedrich-Wilhelms-Universität Bonn, Wegelerstraße 6, 53115 Bonn, Germany, sergio.conti@uni-bonn.de

†Department of Mathematics, University of Duisburg-Essen, Lotharstr. 65, D-47048 Duisburg, Germany, {held}{pach}{schultz}@math.uni-duisburg.de

‡Institute for Numerical Simulation, Rheinische Friedrich-Wilhelms-Universität Bonn, Nussallee 15, 53115 Bonn, Germany, martin.rumpf@ins.uni-bonn.de

However, in various practical applications, there are possible realizations of the random variables that are rather unlikely but which, in case they do occur, have catastrophic consequences. Because of their low probability such scenarios would not have a significant impact on the expectation value. This motivates the development of risk-averse optimization models which are more sensitive against such harmful but unlikely events. The stochastic programming point of view enables us to investigate such *risk averse models*. In this paper, we refine the risk measurement and consider the expectation with respect to suitable nonlinear functions of the cost for each stochastic realization. In particular, we address the expected excess, which reflects the expectation of the costs exceeding a given threshold, or the excess probability, which measures the probability of a failure, i. e. of a realization with a cost value above the threshold value. These models have already been studied in the context of finite dimensional two–stage stochastic programming.

Before we discuss our model, let us briefly review some more recent approaches in shape optimization which already generalize the single load assumption. In so–called multiload approaches a fixed (usually small) number of different loading configuration is considered and optimization refers to this set of configurations, see, e.g., [5, 23, 46] and references therein. In these approaches each evaluation of the objective functional requires a separate computation for each of the possible stochastic forces, which renders them infeasible if the set of possible forces is large, as for example is the case when one aims at approximating a continuous distribution of forces. A more efficient method was derived for a truss model in [8], where it is shown that optimization of the expected compliance is equivalent to a convex problem, and hence efficiently solvable. This however is based on additional geometrical assumptions, namely, on considering a fixed *ground structure*, and leaving only the thickness of the bars to be optimized. Compared to these approaches, which require an evaluation of the objective function for each realization of the stochastic loading, we confine to the evaluation of basis modes for the surface and volume loading. Furthermore, in multiload optimization one basically optimizes the average cost functional and not the expectation of nonlinear risk measures acting on the cost functional. A robust probabilistic approach for the optimization of simple beam models is discussed in [1], whereas in [28] structural reliability is discussed for beam geometries with uncertain load magnitude. Worst-case situations in a multiload context have also been considered, see, e.g., [11]. Structural optimization under incomplete information is also addressed in [10]. The authors investigate different types of uncertainties and follow a non-probabilistic, robust worst case approach. They work out effective techniques to transform optimal design problems with uncertainties into conventional structural optimization problems. In [36] a worst case analysis for given bounds on uncertain loads has been implemented based on a boundary element approach. A worst case compliance optimization is investigated in [6] based on a level set description of shapes and a semi–definite programming approach in the minimization algorithm.

Our approach on nonlinear risk measures and an effective minimization algorithm builds upon previous work on an expectation-based model in [17].

The paper is organized as follows. We will review risk measures in the context of finite dimensional stochastic programming in Section 2 to familiarize ourselves with the general concept and the corresponding two-stage stochastic programming paradigm. In Section 3 we briefly introduce the elastic state equation and define suitable cost functionals for a fixed realization of the loading. A general class of risk-averse shape-optimization models, and the examples of expected excess and excess probability, as well as proper smooth approximations, are presented in Section 4. Section 5 gives a compact description of the level set representation of elastic shapes and the relaxation scheme via a regularized gradient descent. In particular, we will see how to use basis loads and a corresponding basis of primal and dual solutions to compute the shape gradient efficiently even in the presence of a large number of realizations of the stochastic loading. Furthermore, stochastic topology optimization is considered in Section 6. Section 7 describes our numerical algorithm. In Section 8 computational results are presented and we relate qualitative properties of risk averse optimal shapes to corresponding observation in the context of finite dimensional programming.

2 Review of risk averse stochastic programming

Two-stage stochastic programming aims at optimizing nonanticipative decisions which arise in a two-stage scheme of alternating decision and observation. As a paradigmatic example consider the linear case in finite dimension. Here we have a random optimization problem

$$\min \left\{ c^T x + q^T y : Tx + Wy = z(\omega), \, x \in X, \, y \in Y \right\}, \tag{1}$$

where X, Y are polyhedra in Euclidean space and randomness is indicated by the dependence on a random outcome ω in a probability space Ω. We require that x has to be nonanticipative which is expressed by the information constraint

$$\text{decide } x - \quad \text{observe } \omega - \quad \text{decide } y = y(x, \omega).$$

This motivates to rewrite (1) as

$$\min_x \left\{ c^T x + \min_y \left\{ q^T y : Wy = z(\omega) - Tx, \, y \in Y \right\} : x \in X \right\}. \tag{2}$$

While the inner minimization in the above model, to be executed after decision on x and observation of ω, is well-defined conceptually, the outer is not. Nonanticipativity requires to fix x before knowing the data ω. Deriving, from this departure point, conceptually sound optimization models is a central issue in (finite dimensional) two-stage stochastic programming. To this end consider the random variable $J(x, \omega)$ which, for given $x \in X$, arises as $J(x, \omega) := c^T x + \min_y \left\{ q^T y : Wy = z(\omega) - Tx, \, y \in Y \right\}$. The outer minimization in (2) now can be seen as a minimization over the family of random variables $\{ J(x, \omega) : x \in X \}$. To accomplish this minimization the random variables $J(x, \omega)$ need to be compared. Most commonly this is done by applying statistical parameters of which the expectation is the most popular one. This leads to the well-defined optimization problem

$$\min \left\{ \mathbb{E} \ (J(x, \omega)) : x \in X \right\}.$$

The corresponding expectation based shape optimization model has been introduced in [17]. Of course, this model is risk neutral. Critical realizations of $J(x, \omega)$ with little impact on the expected value are given only little importance. If this is no longer appropriate then a risk averse point of view can be adopted where random variables are compared by risk measures, i.e., statistical parameters reflecting dispersion. In the present paper, we consider two such risk measures, namely the *expected excess* and the *excess probability*. These are defined for a preselected threshold $\eta \in \mathbb{R}$ as follows:

- *expected excess*, i.e. "the expectation of costs exceeding η":

$$\mathbb{E} \left(\max \left\{ J(x, \omega) - \eta, 0 \right\} \right),$$

- *excess probability*, i.e. "the probability of costs exceeding η":

$$\mathbb{P} \left(\left\{ \omega \in \Omega : J(x, \omega) > \eta \right\} \right).$$

The resulting risk-averse shape optimization problems are introduced in Section 4.

In recent years, risk averse approaches to (two-stage) stochastic programming have gained increasing attraction. The monograph [33] offers a broad view into modeling, measuring, and managing risk in (finite dimensional) optimization context. We also refer to its comprehensive list of references. Papers dealing with specific risk averse stochastic programming models include [21, 29, 35, 38], for instance. The conceptual development in the present paper is particularly inspired by [34, 39, 40]. In these articles, risk averse linear two-stage stochastic programs derived from (2) were studied. Genuinely finite dimensional solution techniques, such as cutting plane methods from convex optimization or Lagrangean relaxation of mixed-integer programs, constitute the algorithmic pillars there.

3 State equations and cost functionals

Our aim is to optimize the shape of an elastic body $\mathcal{O} \subset \mathbb{R}^d$ ($d = 2, 3$) subjected to internal and external forces. We consider admissible shapes $\mathcal{O}$ which are subsets of a fixed, bounded working domain $D \subset \mathbb{R}^d$. The boundary $\partial\mathcal{O}$ is assumed to be partitioned into Γ_D, Γ_N, and Γ_0. Here Γ_D is a fixed Dirichlet boundary of positive capacity, and Γ_N is a fixed Neumann boundary. On the remaining set Γ_0, which we effectively optimize, we assume homogeneous Neumann boundary conditions. In order to keep the Dirichlet and Neumann boundaries fixed, we shall choose an open set $\mathcal{O}_* \subset D$ such that $\Gamma_D, \Gamma_N \subset \partial\mathcal{O}_* \setminus \partial D$, and restrict the class of admissible shapes to those open sets $\mathcal{O}$ such that $\mathcal{O}_* \subset \mathcal{O} \subset D$. Then necessarily $\Gamma_D, \Gamma_N \subset \partial\mathcal{O}$.

We assume that a random variable ω follows a discrete distribution with scenarios ω_i and probabilities π_i with $i = 1, \dots, N_s$ ($\sum_{i=1}^{N_s} \pi_i = 1$); continuous distributions can be recovered in the limit $N_s \to \infty$. For a given admissible shape $\mathcal{O} \subset \mathbb{R}^2$ the elastic displacement $u = u(\mathcal{O}, \omega) \colon \mathcal{O} \to \mathbb{R}^d$ is assumed to minimize the functional

$$E(\mathcal{O}, u, \omega) := \frac{1}{2} A(\mathcal{O}, u, u) - l(\mathcal{O}, u, \omega), \tag{3}$$

with $A(\mathcal{O}, \zeta, \theta) := \int_{\mathcal{O}} A_{ijkl} e_{ij}(\zeta) e_{kl}(\theta)\, dx$ and $l(\mathcal{O}, \zeta, \omega) := \int_{\mathcal{O}} f(\omega) \cdot \zeta\, dx + \int_{\Gamma_N} g(\omega) \cdot \zeta\, d\mathcal{H}^{d-1}$, among all $u \in H^1_{\Gamma_D}(\mathcal{O}; \mathbb{R}^d) := \{u \in H^1(\mathcal{O}; \mathbb{R}^d) : u = 0 \text{ on } \Gamma_D\}$. Note that we implicitly sum over repeated indices. Here $e(u) = \frac{1}{2}(\nabla u + \nabla u^T)$ denotes the linearized strain tensor, and $A = (A_{ijkl})_{ijkl}$ the elasticity tensor, e. g. for an isotropic material $A_{ijkl} = 2\mu\delta_{ik}\delta_{jl} + \lambda\delta_{ij}\delta_{kl}$ with Lamé coefficients $\lambda, \mu > 0$. Furthermore, we suppose for the volume force $f(\omega) \in L^2(D; \mathbb{R}^d)$ and for the surface load $g(\omega) \in L^2(\Gamma_N; \mathbb{R}^d)$. For fixed realization ω, the minimization of the energy is equivalent to the solution of $-\operatorname{div}(Ae(u)) = f(\omega)$ with appropriate boundary conditions involving $g(\omega)$.

For the shape optimization we consider a general objective functional $\mathbf{J}$ which depends on both the shape $\mathcal{O}$ and the resulting elastic displacement $u(\mathcal{O})$, and is given by

$$\mathbf{J}(\mathcal{O}) := J(\mathcal{O}, u(\mathcal{O})) = \int_{\mathcal{O}} j(u(\mathcal{O}))\, dx + \int_{\partial\mathcal{O}} k(u(\mathcal{O}))\, d\mathcal{H}^{d-1}. \tag{4}$$

For a later efficient numerical realization in case of a high number of stochastic realizations of the loading we restrict here to linear or quadratic functions $j(.)$ and $k(.)$. In the deterministic case of a single realization of the loading we consider $\min\{\mathbf{J}(\mathcal{O}) : \mathcal{O} \in \mathcal{U}_{\mathrm{ad}}\}$ on a set of admissible shapes $\mathcal{U}_{\mathrm{ad}}$. As particular instances of the general objective functional (4), we take into account the compliance

$$\mathbf{J}_1(\mathcal{O}) := l(\mathcal{O}, u(\mathcal{O})) = \int_{\mathcal{O}} f \cdot u(\mathcal{O})\, dx + \int_{\Gamma_N} g \cdot u(\mathcal{O})\, d\mathcal{H}^{d-1}, \tag{5}$$

and the least square error compared to a target displacement u_0

$$\mathbf{J}_2(\mathcal{O}) := \frac{1}{2} \int_{\mathcal{O}} |u - u_0|^2\, dx. \tag{6}$$

In both cases we usually include an penalty for the object volume $\alpha \int_{\mathcal{O}} dx$ with $\alpha \geq 0$.

The shape derivative [19] of the objective functional $\mathbf{J}$ in the direction v initially takes the form $\mathbf{J}'(\mathcal{O})(v) = J_{,\mathcal{O}}(\mathcal{O}, u(\mathcal{O}))(v) + J_{,u}(\mathcal{O}, u(\mathcal{O}))(u'(\mathcal{O})(v))$. To avoid an evaluation of $u'(\mathcal{O})(v)$ for any test vector field v, one introduces the dual or adjoint problem. In fact, the dual solution $p = p(\mathcal{O}, \omega_i) \in H^1_{\Gamma_D}(\mathcal{O}; \mathbb{R}^d)$ is defined as the minimizer of the dual functional

$$E_{dual}(\mathcal{O}, p) := \frac{1}{2} A(\mathcal{O}, p, p) + l_{dual}(\mathcal{O}, p),$$

with $l_{dual}(\mathcal{O}, p) = \int_{\mathcal{O}} j'(u)p\, dx + \int_{\partial\mathcal{O}} k'(u)p\, d\mathcal{H}^{d-1}$. For the compliance objective (5) we observe that $p = -u$. Given p for fixed u and $\mathcal{O}$ we can evaluate the shape derivative of the deterministic cost functional as follows:

$$\mathbf{J}'(\mathcal{O})(v) = J_{,\mathcal{O}}(\mathcal{O}, u(\mathcal{O}))(v) - l_{,\mathcal{O}}(\mathcal{O}, p(\mathcal{O}))(v) + A_{,\mathcal{O}}(\mathcal{O}, u(\mathcal{O}), p(\mathcal{O}))(v) \tag{7}$$
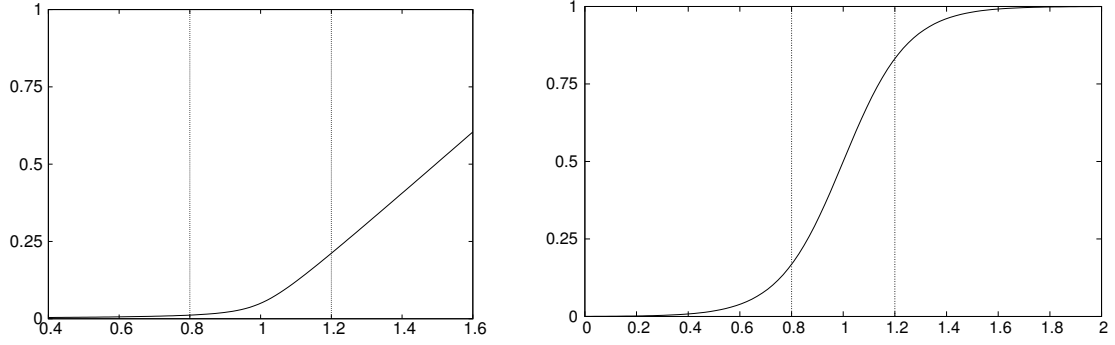
4

Figure 1: The profiles of q^ϵ with $\epsilon = 0.01$ (left) and H^ϵ for $\epsilon = 0.25$ for $\eta = 1.0$ as they are used in the applications in Section 8 below.

$$= \int_{\mathcal{O}} (v \cdot n) \big[j(u(\mathcal{O})) - (f + g\, h + \partial_n g)\, p(\mathcal{O}) + A_{ijkl} e_{ij}(u(\mathcal{O})) e_{kl}(p(\mathcal{O})) \big] \mathrm{d}\mathcal{H}^{d-1} \,.$$

where h denotes the mean curvature of $\partial\mathcal{O}$. For further details we refer to [19, 45] and in case of the particular application to [17].

4 Risk averse shape optimization models

We replace a minimization of the expectation of the objective function by a minimization of the expectation of a nonlinear monotone increasing function of the objective function. This reflects a refined measurement of the effective risk. Indeed it permits to increase the relative weight of unlikely but large values of the objective function. We shall in particular focus the expected excess and the excess probability as risk measures (cf. Section 2) and investigate suitable smooth approximations of the latter. Thus, we ask for shapes $\mathcal{O}$ which minimize

$$\mathbf{Q}(\mathcal{O}) := \mathbb{E}\left(q(J(\mathcal{O}, \omega)) \right) = \sum_{i=1}^{N_s} \pi_i q(J(\mathcal{O}, \omega_i)) \tag{8}$$

where $q : \mathbb{R} \to \mathbb{R}$ is a monotone function. For $q(t) = t$ this reduces again to a minimization of the expected value.

Expected Excess. In analogy to finite dimensional stochastic programming (cf. Section 2), we define here a stochastic shape-optimization problem using the expected excess risk measure. Given a preselected tolerance level $\eta \in \mathbb{R}$, and using the weight function $q(t) = \max\{t - \eta, 0\}$, we obtain the expected excess:

$$\mathbf{Q}_{\mathrm{EE}_\eta}(\mathcal{O}) := \mathbb{E}\left(\max\{J(\mathcal{O}, \omega) - \eta, 0\} \right) \,.$$

For practical convenience we will replace the max-function by a smooth approximation

$$\mathbf{Q}^\epsilon_{\mathrm{EE}_\eta}(\mathcal{O}) = \mathbb{E}\left(q^\epsilon(J(\mathcal{O}, \omega)) \right)$$

where $q^\epsilon(t) := \frac{1}{2}\left(\sqrt{(t - \eta)^2 + \epsilon} + (t - \eta) \right)$ (cf. Fig. 1).

Excess Probability. Correspondingly, if we model the risk measure of excess probability for a preselected tolerance level $\eta \in \mathbb{R}$ now using the weight function $q(t) = H(t - \eta)$ where H denotes the Heaviside function with $H(t) = 1$ for $t > 0$ and 0 otherwise, we get the excess probability:

$$\mathbf{Q}_{\mathrm{EP}_\eta}(\mathcal{O}) := \mathbb{E}\left(H\left(J(\mathcal{O}, \omega) - \eta \right) \right) \,.$$

A suitable smooth approximation is given by

$$\mathbf{Q}^\epsilon_{\mathrm{EP}_\eta}(\mathcal{O}) = \mathbb{E}\left(H^\epsilon(J(\mathcal{O}, \omega)) \right)$$

5

for $H^\epsilon(t) := \dfrac{1}{1 + e^{-\frac{2t}{\epsilon}}}$ (cf. Fig. 1).

5 Level set based gradient descent

In this section we discuss the representation via a level set function ϕ of the shape $\mathcal{O}$ undergoing the optimization procedure. We in particular discuss a spatially continuous descent strategy for a given risk measure, and a particular cost functional based on a regularized gradient descent for this level-set representation. This requires in particular to specify the shape derivative of the risk measure.

Level set description of shapes. We identify the shape $\mathcal{O} \subset D$ with a level set function ϕ on the underlying computational domain D as follows. The shape $\mathcal{O}$ itself consists of the set of points $x \in D$ with $\phi(x) < 0$, the shape contour is the zero level set of ϕ, and finally $\phi(x) > 0$ corresponds to the complement of $\bar{\mathcal{O}}$ on the computational domain D. The well-known level set equation [31, 30] can be interpreted as relation between variations s of the level set function ϕ and normal variations $(v \cdot n)\, n$ of the underlying shape given by $s = -\nabla \phi\, v$. Here, $n := -\frac{\nabla\phi}{|\nabla\phi|}$ denotes the outward pointing normal vector field to $\partial \mathcal{O} = \phi^{-1}(0)$. Given this identification, we can rewrite the cost functional $\mathbf{J}$ in a straightforward manner in terms of the level set function ϕ. Hence, we define $\mathcal{J}(\phi,\omega_i) := \mathbf{J}(\{\phi < 0\}, \omega_i)$ and obtain $\mathcal{J}'(\phi,\omega_i)(s) = \mathbf{J}'(\{\phi < 0\}, \omega_i)\left(-s\, |\nabla\phi|^{-1} n\right)$ for the shape derivative of $\mathcal{J}$. Thus, for our general objective functional (4) we deduce from (8) that

$$
\begin{aligned}
\mathcal{J}'(\phi,\omega_i)(s) = &-\int_{\partial\mathcal{O}} \frac{s}{|\nabla\phi|}\big[j(u(\mathcal{O},\omega_i)) - (f_i + g_i\, h + \partial_n g_i)\, p(\mathcal{O},\omega_i) \\
&+ A_{ijkl} e_{ij}(u(\mathcal{O},\omega_i)) e_{kl}(p(\mathcal{O},\omega_i))\big]\ \mathrm{d}\mathcal{H}^{d-1}\,,
\end{aligned}
\tag{9}
$$

where h denotes the mean curvature, given by $h = \operatorname{div}\left(-\frac{\nabla\phi}{|\nabla\phi|}\right)$.

Shape derivatives of the risk measures. In our risk averse optimization context the cost functional acts as the argument of the nonlinear risk measure function q (cf. Section 4). By the chain rule, we next compute the shape derivative of the stochastic risk measure $\mathcal{Q}(\phi)$ defined, in analogy to (8), by $\mathcal{Q}(\phi) := \mathbb{E}(q(\mathcal{J}(\phi,\omega)))$, and obtain

$$
\mathcal{Q}'(\phi)(s) = \sum_{i=1}^{N_s} \pi_i\, q'(\mathcal{J}(\phi,\omega_i))\, \mathcal{J}'(\phi,\omega_i)(s)\,.
\tag{10}
$$

Let us denote by $\mathcal{Q}^\epsilon_{\mathrm{EE}_\eta}(\phi) = \mathbf{Q}^\epsilon_{\mathrm{EE}_\eta}(\mathcal{O})$ and $\mathcal{Q}^\epsilon_{\mathrm{EP}_\eta}(\phi) = \mathbf{Q}^\epsilon_{\mathrm{EP}_\eta}(\mathcal{O})$ the approximated expected excess and excess probability, respectively, acting on a level set function ϕ. Then we obtain for these risk measures:

$$
\begin{aligned}
\left(\mathcal{Q}^\epsilon_{\mathrm{EE}_\eta}\right)'(\phi)(s) &= \sum_{i=1}^{N_s} \frac{\pi_i}{2}\mathcal{J}'(\phi;\omega_i)(s)\left[\frac{\mathcal{J}(\phi,\omega_i) - \eta}{\sqrt{(\mathcal{J}(\phi,\omega_i) - \eta)^2 + \epsilon}} + 1\right]\,, \\
\left(\mathcal{Q}^\epsilon_{\mathrm{EP}_\eta}\right)'(\phi)(s) &= \sum_{i=1}^{N_s} \frac{2}{\epsilon}\pi_i \mathcal{J}'(\phi,\omega_i)(s)\, e^{-\frac{2}{\epsilon}(\mathcal{J}(\phi,\omega_i)-\eta)}\left(1 + e^{-\frac{2}{\epsilon}(\mathcal{J}(\phi,\omega_i)-\eta)}\right)^{-2}\,.
\end{aligned}
$$

Evaluation of the variation of the cost functional. So far, it seems that for every realization one has to compute a primal solution $u(\mathcal{O},\omega_i)$ and a dual solution $p(\mathcal{O},\omega_i)$. Under our assumption that $j(\cdot)$ and $k(\cdot)$ are linear or quadratic functions, there is a significant algorithm shortcut at our disposal for $N_s \gg 1$, which we will recall here. For details we refer to [17]. Let us assume that there is a small number of (deterministic) basis volume forces $f_1,\ldots,f_{K_1} \in L^2\left(D;\mathbb{R}^2\right)$, and of (deterministic) basis surface loads $g_1,\ldots,g_{K_2} \in H^1\left(D;\mathbb{R}^2\right)$. Then, the actual loads $f(\omega)$ and $g(\omega)$, respectively, are given as linear combinations of these deterministic basis loads $f(\omega) = \sum_{i=1}^{K_1} c^f_i(\omega) f_i$ and $g(\omega) = \sum_{j=1}^{K_2} c^g_j(\omega) g_j$, with the uncertain coefficients $c^f_i(\omega) \in \mathbb{R}$, $i = 1,\ldots,K_1$,

and $c_j^g(\omega) \in \mathbb{R}$, $j = 1, \ldots, K_2$. The advantage of this approach is that we only need to solve as many elasticity PDEs as there are scenarios in order to evaluate the objective functional for a given shape $\mathcal{O}$. This will reduce the computing cost significantly in case $N_s \gg K_1 + K_2$. Suppose $u^{(i\,0)}$ is the elastic displacement for given volume force $f := f_i$ and surface load $g := 0$, for all $i = 1, \ldots, K_1$. Similarly, let $u^{(0\,j)}$ be the displacement corresponding to the volume force $f := 0$ and the surface load $g := g_j$, for all $j = 1, \ldots, K_2$. Then,

$$\bar{u}\,(\mathcal{O}; \omega) := \sum_{i=1}^{K_1} c_i^f(\omega) u^{(i\,0)} + \sum_{j=1}^{K_2} c_j^g(\omega) u^{(0\,j)} \tag{11}$$

is the minimizer of (3) with volume force $f := f(\omega)$, and surface load $g := g(\omega)$. A similar relation holds for the adjoint state $\bar{p}\,(\mathcal{O}; \omega)$ in scenario ω, if we additionally assume that $\sum_{i=1}^{K_1} c_i^f(\omega) + \sum_{j=1}^{K_2} c_j^g(\omega) = 1$, which can always be achieved by choosing the basis forces appropriately. In that case, and if we denote the adjoint states for the individual basis forces by $p^{(i\,0)}$ and $p^{(0\,j)}$, one can see that

$$\bar{p}\,(\mathcal{O}; \omega) := \sum_{i=1}^{K_1} c_i^f(\omega) p^{(i\,0)} + \sum_{j=1}^{K_2} c_j^g(\omega) p^{(0\,j)} \tag{12}$$

is the adjoint state belonging to the state $\bar{u}\,(\mathcal{O}; \omega)$. Here, we also used the fact that the cost functional $\mathcal{J}(\mathcal{O}, \cdot)$ is a quadratic polynomial.

Regularized grad flows. In order to minimize a particular risk measure $\mathcal{Q}$, we consider a gradient descent

$$\phi(t) = -\operatorname{grad}_{\mathcal{G}} \mathcal{Q}(\phi)$$

with respect to the regularizing metric $\mathcal{G}(\zeta, \xi) = \int_D \zeta\xi + \frac{\sigma^2}{2}\,\zeta \cdot \,\xi\,\mathrm{d}x$, which leads to a smooth extension of the shape gradient onto the vicinity of the shape boundary $\mathcal{O}$. Indeed, it corresponds to the application of the inverse of a linear Helmholtz operator to the shape gradient.

6 Topological derivative for risk averse models

A descent procedure based on the shape derivative alone is not, in general, capable of changing the topology of the shape. In some cases the resulting optimal shape strongly depends on this choice of the initial topology (cf. [4, 7, 17]). Although a level-set description of the optimal shape entails no restriction on the topology, the evolution of a level set based on a gradient flow is only able to merging existing holes together, and not capable of creating new holes. The so-called "bubble method" or *topological sensitivity* is based on the idea of testing the target functional with small holes of prescribed shape and computing an asymptotic expansion depending on the radius ρ. It has been introduced by Schumacher [41] for the case of compliance minimization. The method was generalized to a wider class of shape functionals by Sokolowski and Zokowski [42] and applied to 3D elasticity in [43]. In [44], the approach is extended to the case of finitely many circular holes, combining topology variations with boundary variations simultaneously. Using an adjoint method and a truncation technique, Garreau et al. [22] computed the topological sensitivity for general objective functionals and arbitrarily-shaped holes. The topological derivative has been incorporated into the level set method, e.g. in [14], and also combined with the shape derivative in that context (cf. e.g. [4, 9, 25]). Notice that even including the topological derivative the optimization remains local, hence the numerical solution can only be expected to converge to a local minimum, which is not necessarily a global one (cf. Figures 2 and 7). However, we know that these shapes are local minima with respect to a wider class of perturbations, which also include the creation of holes.

To apply this method in the context of risk averse shape optimization and to start the optimization process with a solid structure we define a stochastic topological gradient based on a weighted sum of topological gradients for the different scenarios. For the single scenario case we follow Garreau

et al. [22]. Suppose we aim at minimizing the functional $\mathbf{J}(\mathcal{O})$. Let $\mathcal{O}_\rho := \mathcal{O} \setminus \left(x + \overline{\rho\mathfrak{M}} \right)$ be the perforated domain obtained removing a small part $\mathfrak{M}_\rho := x + \rho\mathfrak{M}$ from $\mathcal{O}$ for a fixed open bounded set $\mathfrak{M} \subset \mathbb{R}^2$. Then, under appropriate smoothness assumptions one obtains an asymptotic expansion of $\mathbf{J}$:

$$\mathbf{J}(\mathcal{O}_\rho) = \mathbf{J}(\mathcal{O}) + \mathbf{f}(\rho)\,\mathbf{D}_{\text{topo}}\mathbf{J}(x) + o\left(\mathbf{f}(\rho)\right),$$

where $\mathbf{f}$ is a smooth function with $\lim_{\rho \to 0} \mathbf{f}(\rho) = 0$, and $\mathbf{f}(\rho) > 0$. The quantity $\mathbf{D}_{\text{topo}}\mathbf{J}(x)$ is called *topological gradient* at the point $x \in \mathcal{O}$. It is here important that the objective function $\mathbf{J}(\mathcal{O}_\rho)$ is computed with the elastic displacement u_ρ which minimizes the elasticity problem (3) on the domain $\mathcal{O}_\rho$. Thus, the topological derivative $\mathbf{D}_{\text{topo}}\mathcal{Q}$ of the objective function $\mathcal{Q}(\phi) = \mathbb{E}(q(\mathbf{J}(\mathcal{O},\omega)))$ at a point $x \in \mathcal{O}$ provides information about the effect of creating a small hole located at x, and can thus be used like a descent direction in the optimization process. From now on, we take $\mathfrak{M}$ to be the unit ball. For any $x \in \mathcal{O}$, the topological derivative of the risk averse cost functional is computed by the chain rule as

$$\mathbf{D}_{\text{topo}}\mathcal{Q}(x) = \sum_{i=1}^{N_s} \pi_i\, q'(\mathbf{J}(x,\omega_i))\mathbf{D}_{\text{topo}}\mathbf{J}(x,\omega_i)$$

where $\mathbf{D}_{\text{topo}}\mathbf{J}$ is the slope of the cost in case of a hole drilling for a single realization. Then, the topological derivative for the compliance $\mathbf{J}_1(\mathcal{O})$ defined in (5) and the quadratic functional $\mathbf{J}_2(\mathcal{O})$ defined in (6) for right hand side $f = 0$ are given as follows [43, 22]:

$$\mathbf{D}_{\text{topo}}\mathbf{J}_1(x,\omega_i) = \frac{\pi(\lambda+2\mu)}{2\mu(\lambda+\mu)}\left\{4\mu Ae(u_i):e(u_i) + (\lambda-\mu)\operatorname{tr}(Ae(u_i))\operatorname{tr}(e(u_i))\right\}(x),$$

and the topological derivative of $\mathbf{J}_2$ is given by

$$\begin{aligned}
\mathbf{D}_{\text{topo}}\mathbf{J}_2(x,\omega_i) = &-\frac{\pi}{2}\left(u_i(x) - u_0(x)\right)^2 \\
&-\frac{\pi(\lambda+2\mu)}{4\mu(\lambda+\mu)}\left\{4\mu Ae(u_i):e(p_i) + (\lambda-\mu)\operatorname{tr}(Ae(u_i))\operatorname{tr}(e(p_i))\right\}(x).
\end{aligned}$$

For an effective topology selection in the algorithm we use the topological derivative every n_{top}th step, apply a usual thresholding strategy substracting all points x with $\mathbf{D}_{\text{topo}}\mathcal{Q}(x)$ above the threshold $\theta \max_{y \in \mathcal{O}} \mathbf{D}_{\text{topo}}\mathcal{Q}(y)$ from the shape domain. Fig. 2 illustrates the effectivity but also the sensitivity of the topological derivative. In a cantilever type configuration (a rectangle whose left-hand side is kept fixed, with a tangential force acting on the central part of the right-hand side), where we start with a solid initial shape. Here, we set $\alpha = 0.4$ and used a grid with 513×513 nodes. It is seen that the parameters for the algorithm have to be chosen with care. Inclusion of the topological derivative enhances the algorithm, without, of course, guaranteeing a global optimal solution.
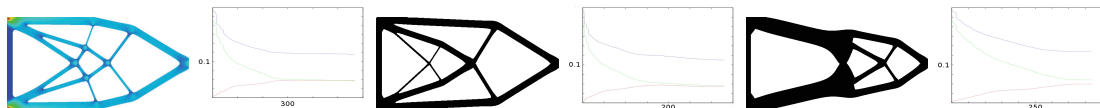

Figure 2: Computational results based on the combined shape derivative and topological derivative approach are depicted for a cantilever problem with deterministic loading. We choose $n_{top} = 15$, $\theta = 0.9$ (left), $n_{top} = 5$, $\theta = 0.9$ (middle), and $n_{top} = 15$, $\theta = 0.95$ (right). The resulting shape color coded by the von Mises stress as ▮▮▮▮ and a plot of the objective function (blue, top), the enclosed volume (green, middle), and the compliance functional (red, bottom) over the iterations of the algorithm are shown. The middle shape has the slightly better objective value 0.111 than the left one with 0.117. The third shape, which already looks strikingly different has the (worst) objective value 0.129

7 Numerical algorithm

In this section we detail the concrete numerical algorithm in two space dimensions ($d = 2$) and discuss our finite element approach for the representation of the level set function on the working domain D, and suitable finite elements spaces for the primal and the dual solutions. Furthermore, we show how to combine the topological derivative and the regularized gradient descent approaches in a robust discrete-energy minimization.

Finite element discretization. For the ease of implementation we restrict ourselves to the working domain $D = [0, 1]^2$. We suppose that the usual dyadic grid hierarchy consisting of squares is generated, each of these squares is supposed to be divided along one of the diagonals into two triangles. On each of these triangular grids we consider the space $\mathcal{V}_h$ of piecewise affine, continuous functions, where $h = 2^l$ denotes the grid size on level l of the grid hierarchy. A discrete level set function $\Phi \in \mathcal{V}_h$ identifies a discrete, polygonally bounded elastic body $\mathcal{O}_h = \{x \in D : \Phi(x) < 0\}$. Here, we explicitly work with a void phase $D \setminus \mathcal{O}$ and, at variance with [4, 3], we do not consider a softer elastic material outside of the actual elastic body $\mathcal{O}$ to be optimized. Thus, we have to define suitable finite element spaces on the discrete elastic domain $\mathcal{O}_h$. To avoid a complicated regular remeshing of the boundary $\mathcal{O}_h$ [20, 32] we resort to composite finite elements. They have been introduced by Hackbusch and Sauter [24] and allow for efficient multigrid solvers for elliptic problems on complicated domains. In fact, given a basis function $\Theta_i \in \mathcal{V}_h$ whose support intersects the discrete elastic domain $\mathcal{O}_h$, we define the corresponding vector-valued composite finite element basis function $\Theta_{ij}^{\mathrm{cfe}}(x) = e_j \, \chi_{\mathcal{O}_h}(x) \, \Theta_i(x)$, where $e_1 = (1, 0)$, $e_2 = (0, 1)$, and $\chi_{\mathcal{O}_h}$ denotes the characteristic function of the discrete domain $\mathcal{O}_h$. Collecting all those basis functions which vanish on the Dirichlet boundary we obtain the composite finite element space $\mathcal{V}_h^{\mathrm{cfe}}$. Notice that to conserve the Dirichlet boundary condition we furthermore freeze the level set function Φ on the set $\mathcal{O}_*$, which can be interpreted as a small neighbourhood of the Dirichlet boundary Γ_D and the Neumann boundary Γ_N on which the surface load is applied (see discussion at the beginning of Section sec:statecost). Hence, in this region the body still behaves elastically, but does not undergo any optimization.

Discrete primal and dual solutions. For a given basis load the discrete primal solution is defined as the finite element function $U^{i\,j} \in \mathcal{V}_h^{\mathrm{cfe}}$ solving $A(\mathcal{O}_h, U^{i\,j}, \Theta) = l^{i\,j}(\mathcal{O}_h, \Theta)$ for all $\Theta \in \mathcal{V}_h^{\mathrm{cfe}}$, where $l^{i\,0}(\mathcal{O}_h, \Theta) := \int_{\mathcal{O}_h} f_i \cdot \Theta \, \mathrm{d}x$ and $l^{0\,j}(\mathcal{O}_h, \Theta) := \int_{\mathcal{O}_h} g_j \cdot \Theta \, \mathrm{d}\mathcal{H}^{d-1}$ for $1 \leq i \leq K_1$ and $1 \leq j \leq K_2$. The corresponding set of dual solutions are those functions $P^{i\,j} \in \mathcal{V}_h^{\mathrm{cfe}}$, for which $A(\mathcal{O}_h, \Theta, P^{i\,j}) = -J_{,u}(\mathcal{O}_h, U^{i\,j})(\Theta)$. for all $\Theta \in \mathcal{V}_h^{\mathrm{cfe}}$. Due to the assumption on $J(\mathcal{O}, \cdot)$ the integrand is at most quadratic and can be integrated exactly using a Gauss quadrature rule. Finally, for loads $f(\omega_i)$ and $g(\omega_i)$ take into account the linear factors of the different basis loads and compute $\bar{U}(\mathcal{O}_h, \omega_i)$, $\bar{U}(\mathcal{O}_h, \omega_i)$ for $i = 1, \ldots, N_S$ according to the discrete analog of (11) and (12), respectively. For further details on the primal and dual solutions we refer to [17] and for the composite finite element approach in the context of domains described via level sets we refer to [27].

Discrete gradient descent algorithm. The numerical relaxation of the shape functional is based on the time discretized, regularized gradient descent scheme given in (13) combined with intermediate topology optimization steps and applied to the spatially discrete stochastic shape functional

$$\mathcal{Q}(\Phi) := \mathbb{E}\left(q(\mathcal{J}(\Phi, \omega)) \right) = \sum_{i=1}^{N_s} \pi_i q(\mathcal{J}(\Phi, \omega_i)).$$

The regularized gradient descent scheme computes for an initial discrete level set function $\Phi^0 \in \mathcal{V}_h$ a sequence of level set functions $(\Phi^k)_{k=1}$ based on

$$\mathcal{G}(\Phi^{k+1} - \Phi^k, S) = -\tau \mathcal{Q}'(\Phi^k, \omega)(S) \tag{13}$$

9

for given time step τ and all $S \in \mathcal{V}_h$. Hence, the vector

$$\mathcal{Q}'(\Phi^k, \omega)(S) = \sum_{i=1}^{N_s} \pi_i\, q'(\mathcal{J}(\mathcal{O}, \omega_i))\, \mathcal{J}'\left(\Phi^k, \omega_i\right)(S)$$

of variations of the risk measure $\mathcal{Q}$ with respect to all basis functions $S \in \mathcal{V}_h$ has to be computed. Here, we evaluate $\mathcal{J}'\left(\Phi^k, \omega_i\right)(S)$ in analogy to the continuous case in (9). Furthermore, one has to solve the linear system of equations resulting from a standard finite element discretization of $\mathcal{G}$. The time step τ is chosen according to a simple variant of the Armijo step size control. Indeed, given a constant $\beta_* \in (0,1)$ we accept a timestep τ if the condition $\mathcal{Q}(\Phi^{k+1}) - \mathcal{Q}(\Phi^{k+1}) \leq -\frac{\beta_*}{\tau}\mathcal{G}(\Phi^{k+1} - \Phi^k, \Phi^{k+1} - \Phi^k)$ is satisfied, otherwise the timestep is reduced. If the opposite inequality holds for β_* being replaced by some $\beta^* > \beta_*$ we try to widen the timestep.

Intermediate discrete topology optimization. The evolution of the level-set function automatically allows for union of existing holes. The creation of new holes, i.e., the increase in the topological complexity, is instead dealt with through the topological derivative, as discussed in Section 6. Every n_{top} steps we compute the topological derivative $\mathbf{D}_{\text{topo}}\mathcal{Q}(\Phi^k)$, and modify the domain according to its value. In general this procedure does not correspond to creating the infinitesimal holes discussed in Section 6, but rather to creating finite-size holes, which can be well resolved by our grid, and which cover the entire region in which infinitesimal holes would have been convenient. Therefore the usage of the topological derivative should be seen as a quantitative heuristic tool to choose the location and the shape of possible holes; the long-term evolution of those holes is then optimized by the shape derivatives.

Algorithm. Let us collect the ingredients of the fully practical computational scheme in the following sketch of the resulting algorithm.

> **RiskAverseShapeOpt** $\left((f_j, c_j^f(\omega_i)_{i=1}^{N_s})_{j=1}^{K1}, (g_j, c_j^g(\omega_i)_{i=1}^{N_s})_{j=1}^{K2}, (\pi_i)_{i=1}^{N_s}\right)$ {
>   initialize Φ_i in accordance to the boundary conditions on Γ_N, Γ_D;
> $k = 1$; initialize time step τ;
>   do {
>   if ($k \mod n_{\text{top}} = 0$) {
>   compute pointwise topological derivative $\mathbf{D}_{\text{topo}}\mathcal{Q}$;
> $\Phi^k = \text{signdist}\left(\quad ([\Phi^k < 0] \setminus [\mathbf{D}_{\text{topo}}\mathcal{Q}(x) < \theta \max_{y \in \mathcal{O}} \mathbf{D}_{\text{topo}}\mathcal{Q}(y)]\quad \mathcal{O}_*)\right)$;
>   Compute $\bar{U}([\Phi^k < 0], \omega_i)$, $\bar{P}([\Phi^k < 0], \omega_i)$ for $i = 1, \ldots, N_s$ by (11), (12);
>   Compute $\mathcal{Q}'(\Phi^k, \omega)(S)$ by (10);
>   solve the following linear system of equations for Φ^{k+1}:
> $\mathcal{G}(\Phi^{k+1} - \Phi^k, S) = -\tau \mathcal{Q}'(\Phi^k, \omega)(S) \quad S \in \mathcal{V}_h$
>   if $\left(\mathcal{Q}(\Phi^{k+1}) - \mathcal{Q}(\Phi^k) \geq -\frac{\beta_*}{\tau}\mathcal{G}(\Phi^{k+1} - \Phi^k, \Phi^{k+1} - \Phi^k)\right)$ {
> $\tau = \frac{\tau}{2}$; SUCCESS = FALSE
>   }
>   else {
>   SUCCESS = TRUE; $k = k + 1$;
>   if $\left(\mathcal{Q}(\Phi^{k+1}) - \mathcal{Q}(\Phi^k) \leq -\frac{\beta^*}{\tau}\mathcal{G}(\Phi^{k+1} - \Phi^k, \Phi^{k+1} - \Phi^k)\right)$
> $\tau = 2\tau$
>   }
>   } while(SUCCESS *or* $\Phi^k - \Phi^{k-1}$ > Threshold)
> }

For the initial shape represented by Φ_0 a very coarse approximation turns out to be efficient. It should already reflect the boundaries Γ_D and Γ_N including the neighbourhood of Γ_D, which are not effected by the shape optimization. In our applications it turned out that already the first topology optimization step sufficiently adapts the this implicit shape description.
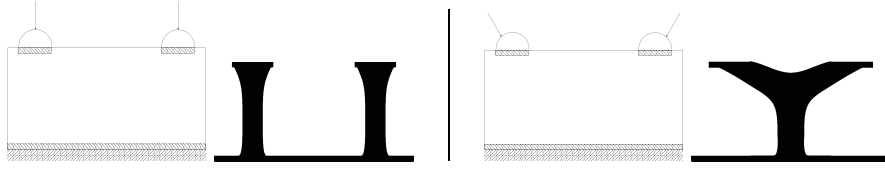
Figure 3: Two different deterministic loading configurations are investigated: vertical loading on the two bearings (left) leads to two disconnected vertical trusses (second left), whereas two non–vertical loads (second right) lead to a Y–shaped truss construction underneath the bearings (right).
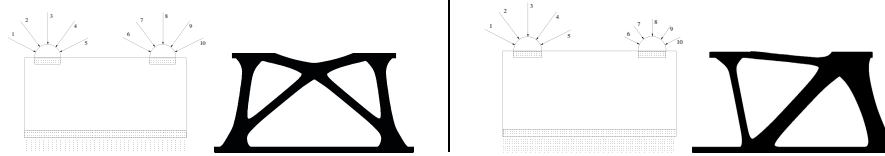

Figure 4: A symmetric stochastic load configuration (left) leads to symmetric support jibs (second left), whereas a nonsymmetric stochastic loading (second right) favors a correspondingly nonsymmetric truss construction.

8   Applications of risk averse shape optimization

In what follows we will discuss two applications. The first one consists of two fixed rectangular bearings, loaded in different directions from the top and we ask for the optical construction of trusses underneath these bearings given a compliance cost functional. In the second example is a cantilever construction, in which we minimize the deflection of a loaded horizontal beam, in the presence of a fixed vertical beam.

All computations are performed on a $\left(2^8 + 1\right) \times \left(2^8 + 1\right)$ grid overlayed the ambient domain $D = [0,1]^2$. Thus, the grid size is $h = 2^{-8}$. The initial time step for the gradient descent scheme is chosen as $\tau = h$ and the parameters for the adaptive time stepping are $\beta^* = 0.5$ and $\beta_* = 0.1$. Every $n_{\text{top}} = 5$ iterations a topology optimization step is performed with $\theta = 0.9$. Furthermore, we have chosen $\epsilon = 0.01$ in the expected excess objective, and $\epsilon = 0.25$ in the excess probability objective. The corresponding regularized max and heaviside functions are depicted in Fig. 1. Finally, for the volume penalty parameter we have chosen $\alpha = 0.5$, and $\sigma = 4h$ in the regularizing metric $\mathcal{G}$.

Trusses underneath two fixed bearings. Before investigating stochastic loading and risk averse shape optimization we consider two different deterministic load configurations: two vertical loads and two oblique loads with vertical average. Fig. 3 shows the corresponding optimal shapes. For each case we report the initial geometry together with the loading configuration and the resulting optimal shape. In the first case the resulting shape is clearly tuned to this specific loading, and would have a very weak response to transversal loadings. Also in the second application, the resulting optimal Y–shape would be far from optimal in a situation with a significant total horizontal force.

We now pass to a stochastic generalization of the same situation, using the expected value objective. In Fig. 4 there are two instances shown, each with 10 scenarios. In the first instance (plotted on the left) all scenarios have identical probabilities and all scenario loads are equally strong. In the second instance (plotted on the right) loads acting on the left bearing are twice as strong as those acting on the right bearing. But the left loads each acts with probability 0.01 while each of the right onces appears with probability 0.19. Hence, the forces on the left play, on average, a minor role. Both configurations require 4 basis forces: two of them have their support only on top of the left bearing, whereas the other two are supported on top of the right bearing. Computational parameters are as above, except that we have set $\alpha = 1$. In Fig. 4 we compare the shapes which minimize the expected value of the compliance cost functional in both cases. As expected the symmetric load configuration leads to a symmetric truss construction, whereas for
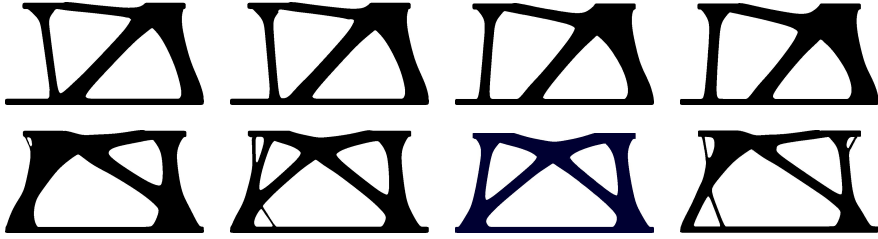
Figure 5: A sequence of results for the optimization with respect to the expected excess for $\eta = 0.1$, 0.2, 0.3, 0.4, 0.6, 0.8, 1.0. , 1.5. The underlying loading is shown in Fig. 4 (second right).
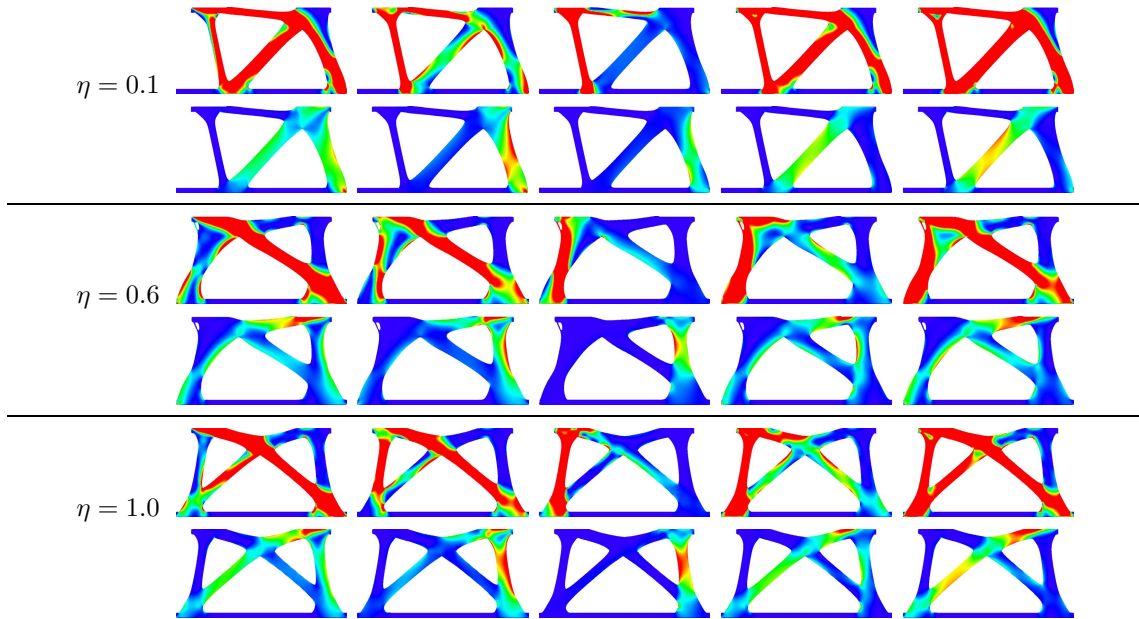

Figure 6: The von Mises stress distributions for the individual scenarios in the optimal shapes with respect to expected excess for different η are colorcoded as ▬▬▬. The stochastic loading is as in Fig. 4 (second right) and the set of realizations is taken from Figure 7. The η values are shown on the left.

nonsymmetric loading nonsymmetric outriggers minimize the expected value of the cost.

Next, we investigate risk averse shape optimization for the second (nonsymmetric) load configuration. In Fig. 5 a family of optimal shapes minimizing the expected excess for varying excess parameter η is depicted. We observe a continuous evolution of the geometry with η, even though each of the computations has been restarted from scratch on the solid bulk domain $\mathcal{O}^* = D$. Due to the nonanticipativity of our stochastic shape optimization model, the actual loading on an optimal shape, but not the shape itself, depends on the load scenario. In Fig. 6 the von Mises stress distribution is colorcoded on the optimal shapes for three different values of η. One clearly sees the significant stresses caused by the strong loading on the left bearing. For the expected excess, scenarios ω for which $J(\mathcal{O}, \omega) \leq \eta$ are irrelevant. In fact, in the regularized formulation of the stochastic cost functional $\mathcal{Q}_{\mathrm{EE}_\eta}^\epsilon$ these scenarios are still taken into account but with very small weights. Therefore, the optimization aims at shapes $\mathcal{O}$ "pushing the objective $J(\mathcal{O}, \omega)$ below η" for the "expensive" scenarios ω, i.e., for the high-probability scenarios acting on the right bearing. This is nicely seen in Fig. 6 where the von Mises stresses always are comparably small for the last five scenarios, i.e., those acting on the right bearing. For growing η value, less and less effort is needed for keeping the objective below η. Therefore less and less material is needed on the right, leaving room for improving the situation on the low-probability scenarios with a strong loading on the left bearing.

Figure 7: In the optimization of the excess probability for $\eta = 0.4$ decreasingly thin trusses are realized on the intermediate grey shape on the left until the left bearing is completely truncated via a topology optimization step (cf. Fig. 4 for the load configuration). The final result is shown on the right.

A strikingly different picture is obtained from the optimization of the excess probability. In this case one observes a complete "mass shift" towards the right bearing. Indeed, since the extent of excess is irrelevant, huge compliances are accepted for the five (low-probability) scenarios on the left as long as it is only possible to keep the objective below η for the (high-probability) scenarios on the right bearing (cf. Fig. 8 for the corresponding cost diagram). As a consequence, no truss construction is needed anymore for the left bearing –correspondingly the numerical relaxation algorithm leads to decreasingly thin connecting trusses. Fig. 7 illustrates the crucial moment in the iterative minimization when the narrow trusses between the bearings are removed via a topology optimization step in order to continue.
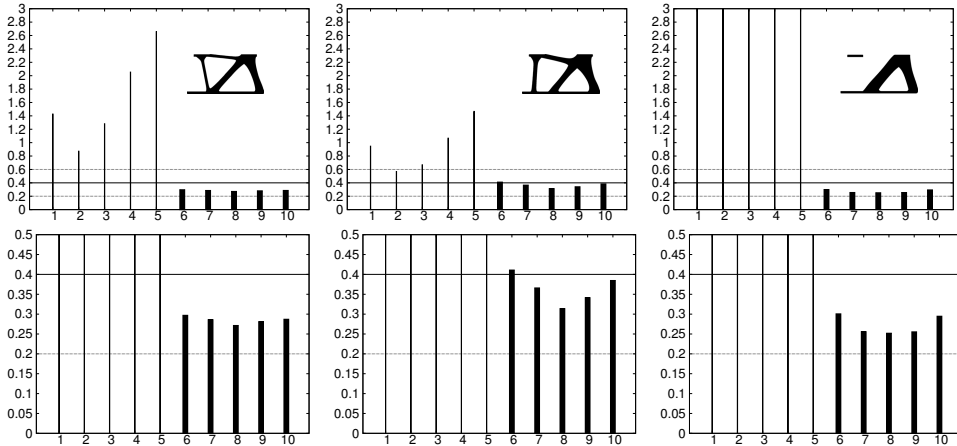

Figure 8: Objective values for each of the 10 scenarios are rendered with bar charts for the optimal shapes corresponding to the stochastic cost functionals $\mathcal{Q}_{EV}$, $\mathcal{Q}_{EE_\eta}^\epsilon$, $\mathcal{Q}_{EP_\eta}^\epsilon$ (from left to the right) for $\eta = 0.4$. The second row shows a zoom into the diagrams. The bar thickness is chosen proportional to the probability.

Figure 8 shows the quantitative difference in the cost distribution over the ensemble of loading scenarios for the different risk averse measures. For the expected value a weighted sum over all single-scenario objectives is minimized. Therefore, the optimization reduces as much as possible the objective values for high-probability scenarios; in contrast for the low-probability scenarios fairly big, but not excessive, values are acceptable. For the expected excess, there is no incentive in optimizing further the scenarios which have an objective value below the threshold, it is instead convenient to use the arising flexibility for decreasing objective values of scenarios above η. For the excess probability it only matters whether the objective value exceeds η or not. This leads to an excessive growth of objective values for scenarios significantly above the threshold, which are expected to be "lost" anyway. In the concrete example, there is no incentive to hold the left bearing, hence it is left floating, sending the corresponding objective value to infinity.

The gained flexibility is now used to push maximal (weighted) scenarios with a cost moderately exceeding η below this threshold. Due to the built–in regularization in $\mathcal{Q}_{EE_\eta}^\epsilon$, $\mathcal{Q}_{EP_\eta}^\epsilon$ the threshold behavior at η is smeared out (cf. Fig. 1 for the actually applied regularization). Thus, cost reduction of single scenarios in the vicinity of the threshold is advantageous with respect to the final regularized expected excess and excess probability.

We finally report the values of the different stochastic cost functionals $\mathcal{Q}_{EV}$, $\mathcal{Q}_{EE_\eta}^\epsilon$, and $\mathcal{Q}_{EP_\eta}^\epsilon$
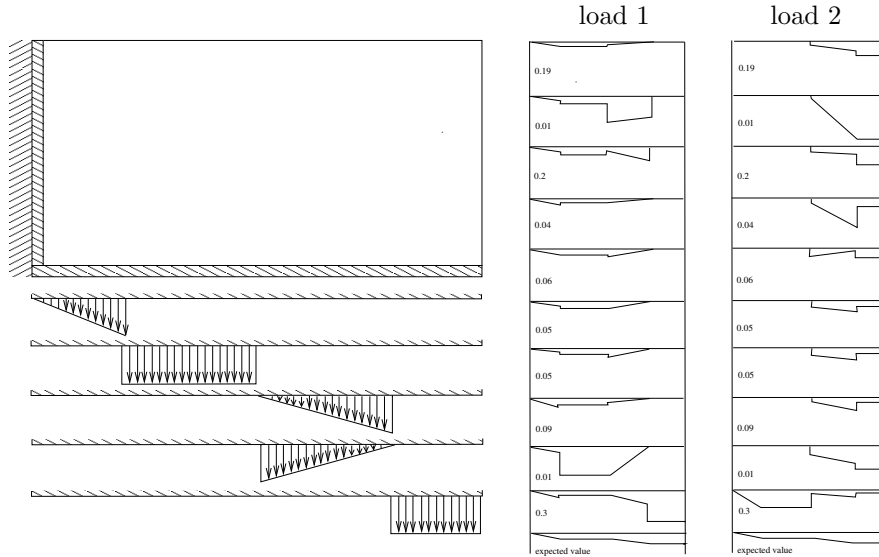
Figure 9: On the initial domain the geometrically fixed lower beam and the vertical beam attaching the cantilever to the wall on the left is displayed on the top left. Underneath the 5 basis loads are depicted and on the right the scenarios of the two different loads are rendered in columns with probabilities associated to each scenario.

on the computed set of optimal shapes $\mathcal{O}_{\mathrm{EE}_\eta}$ (with respect to the expected value), $\mathcal{O}_{\mathrm{EE}_\eta}$ (with respect to the expected excess), and $\mathcal{O}_{\mathrm{EP}_\eta}$ (with respect to the excess probability), respectively, in the following table:

	$\mathcal{Q}_{\mathrm{EV}}$	$\mathcal{Q}_{\mathrm{EE}_\eta}^{\epsilon}$	$\mathcal{Q}_{\mathrm{EP}_\eta}^{\epsilon}$
$\mathcal{O}_{\mathrm{EV}}$	0.293	0.041	0.072
$\mathcal{O}_{\mathrm{EE}_\eta}$	0.368	0.024	0.278
$\mathcal{O}_{\mathrm{EP}_\eta}$	∞	∞	0.068.

Cantilever with geometrically preset, loaded lower beam. The second example is concerned with the optimization of a cantilever construction carrying a horizontal beam, on which vertical surface loads with a random spatial distribution are applied. In fact, we take into account 5 basis loads and two different random loading schemes, each instantiated via 10 different scenarios of varying probability. Fig. 9 depicts the solid block–type initial domain $\mathcal{O}^*$, the basis loads and the scenario ensemble. The expected value of the load is the same in the two loading schemes, as illustrated in the last row of Fig. 9. The cantilever is fixed at a Dirichlet boundary on the left; the thin hedged, vertical layer as well as the hedged horizontal beam are not modified by the shape optimization. For this example we chose as objective functional the squared displacement on the lower beam, which is a measure of the beam deflection. Indeed, we put $j(u) = u^2 + \alpha$. Furthermore, we have $\alpha = 4$; $\eta = 1$ in both configurations. As before we adopt a regularization parameter $\epsilon = 0.01$ for the expected excess applications. For the excess probability the value of ϵ is initially set to 0.5 and then decreased over 0.25 to 0.1 during the optimization procedure.

In this application, a robust relaxation of the risk averse stochastic cost functionals turns out to be much more subtle. Due to the lack of a clear spatial separation of the loading - which appears to be the main difference to our first example - the energy landscape of the stochastic cost functionals is characterized by many local minima. At the same time the structure of the risk functionals generates significant flat regions. We first present our results and then discuss the observed difficulties in more detail. The overall complication is indeed not surprising given the experience in finite dimensional stochastic programming, as we will annotate below. The main differences of the load configurations are as follows:

1. The first loading configuration is characterized by a single, high probability load scenario on the right end of the lower beam.
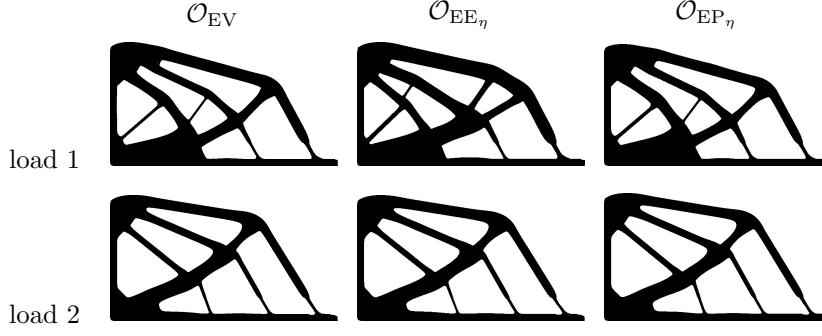
14

$\mathcal{O}_{\mathrm{EV}}$ $\mathcal{O}_{\mathrm{EE}_\eta}$ $\mathcal{O}_{\mathrm{EP}_\eta}$

load 1

load 2

Figure 10: Optimal shapes for the risk averse cost functionals $\mathcal{Q}_{EV}$, $\mathcal{Q}^\epsilon_{EE_\eta}$, and $\mathcal{Q}^\epsilon_{EP_\eta}$ are rendered for the two different random loads (cf. Figure 9).

2. The second configuration has an equal distribution of loads at the right end and a single, high probability load scenario acting on the left half of the lower beam.

The computed optimal shapes for the stochastic cost functionals are shown in Fig. 10, whereas in Fig. 11 we again render the cost distribution onto the different scenarios as bar charts.
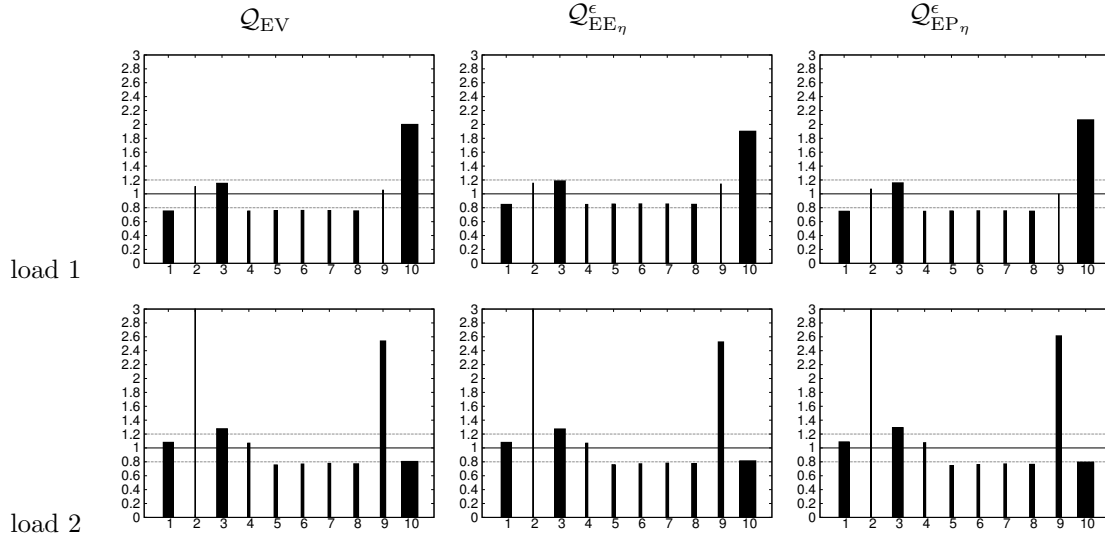

$\mathcal{Q}_{\mathrm{EV}}$ $\mathcal{Q}^\epsilon_{\mathrm{EE}_\eta}$ $\mathcal{Q}^\epsilon_{\mathrm{EP}_\eta}$

load 1

load 2

Figure 11: Bar charts render the objective values for the 10 scenarios for the stochastic cost functionals $\mathcal{Q}_{EV}$, $\mathcal{Q}^\epsilon_{EE_\eta}$, $\mathcal{Q}^\epsilon_{EP_\eta}$ and the different random loads. The bar thickness corresponds to the probability of the corresponding scenario.

In the first load configuration, we observe thicker trusses on the right in case of $\mathcal{Q}^\epsilon_{\mathrm{EE}_\eta}$ compared to $\mathcal{Q}_{\mathrm{EV}}$. For $\mathcal{Q}^\epsilon_{\mathrm{EE}_\eta}$ the construction in the middle is thicker to deal with the load scenarios characterized by strong concentration in this region. The best shape for $\mathcal{Q}^\epsilon_{\mathrm{EE}_\eta}$ differs from that for $\mathcal{Q}_{\mathrm{EV}}$ by a reduced objective value of the high-probability scenario 10 while, at the same time, the values for scenarios 4 to 8 are increased but kept below the threshold of $\eta = 1$. The best shape for $\mathcal{Q}^\epsilon_{\mathrm{EP}_\eta}$, compared to that for $\mathcal{Q}_{\mathrm{EV}}$, permits increase in the value for scenario 10, which is lost anyway, with the benefit of keeping scenario 9 below the threshold.

For the second load configuration, the best shapes for the different stochastic cost functionals differ only little. We will come back to this phenomenon when discussing the difficulties we encountered when running our descent algorithm.

A cross check of the obtained results is compiled in the following tables which list values for the stochastic cost functionals on the set of optimal domains for each of the two different loadings:

1.	$\mathcal{Q}_{\mathrm{EV}}$	$\mathcal{Q}^{\epsilon}_{\mathrm{EE}_\eta}$	$\mathcal{Q}^{\epsilon}_{\mathrm{EP}_\eta}$	2.	$\mathcal{Q}_{\mathrm{EV}}$	$\mathcal{Q}^{\epsilon}_{\mathrm{EE}_\eta}$	$\mathcal{Q}^{\epsilon}_{\mathrm{EP}_\eta}$
$\mathcal{O}_{\mathrm{EV}}$	1.215	0.341	0.511	$\mathcal{O}_{\mathrm{EV}}$	1.021	0.150	0.419
$\mathcal{O}_{\mathrm{EE}_\eta}$	1.240	0.322	0.538	$\mathcal{O}_{\mathrm{EE}_\eta}$	1.022	0.149	0.419
$\mathcal{O}_{\mathrm{EP}_\eta}$	1.233	0.361	0.509	$\mathcal{O}_{\mathrm{EP}_\eta}$	1.021	0.225	0.418

As we already have mentioned above, the energy landscape both of the expected excess functional $\mathcal{Q}_{\mathrm{EE}_\eta}$ and the excess probability functional $\mathcal{Q}_{\mathrm{EP}_\eta}$ is characterized by flat regions. For $\mathcal{Q}_{\mathrm{EE}_\eta}$ these are associated with the scenarios for which $\mathcal{J} < \eta$. For $\mathcal{Q}_{\mathrm{EP}_\eta}$ the energy landscape is completely flat, except on the singular set, where $\mathcal{J} = \eta$ holds for one of the scenarios. By the regularization built into $\mathcal{Q}^{\epsilon}_{\mathrm{EE}_\eta}$ and $\mathcal{Q}^{\epsilon}_{\mathrm{EP}_\eta}$ we theoretically get rid of these degeneracies. As we have seen in the first example this enables a robust and reliable minimization in case of clusters of well separated loads with each load in a cluster of similar impact on the shape. In the cantilever example with its constant expected value of a smoothly distributed stochastic loading, this renders the robust minimization much more difficult.

In particular the usual application of the topological derivative as a marking strategy for regions to be extracted from the current shape - which is obviously a slight abuse of its analytical definition - seems to suffer substantially from the above observations. Indeed, a straightforward minimization of the stochastic cost functionals starting from the initial domain $\mathcal{O}^*$ - as we have successfully performed in the first example - is falling short to fulfill the basic cross check of stochastic cost function values reported in the above tables. For example, in the optimization from scratch for the second stochastic loading case we obtained for the local minimizer $\mathcal{O}_{\mathrm{EP}_\eta}$ the following values for the stochastic cost functionals: $\mathcal{Q}_{\mathrm{EV}} = 1.413$, $\mathcal{Q}^{\epsilon}_{\mathrm{EE}_\eta} = 0.526$, and $\mathcal{Q}^{\epsilon}_{\mathrm{EP}_\eta} = 0.465$. Obviously, this renders the optimal shapes both with respect to the expected value and the expected excess as candidates with lower risk averse stochastic cost than the actually computed local minimizer of the cost functional $\mathcal{Q}^{\epsilon}_{\mathrm{EP}_\eta}$. Thus, in such a case of failure, we have restarted the computation and relaxed the shape for the corresponding cost functional with the shape with the so far lowest cost. Furthermore, the basins of attraction of local minima appear to be small and close by each other. Thus the obtained (local) minimizer of the different stochastic cost functionals vary only slightly.

Related observations in finite dimensional stochastic programming. In two-stage models of finite dimensional stochastic programming, see [37] for a comprehensive reference, the counterparts to the present $J(x, \omega)$ arise as value functions of parametric optimization problems, mostly of parametric linear or mixed-integer linear programs. Then, under mild assumptions, $J(., \omega)$ is convex in the linear case, which clearly extends to the $\mathcal{Q}_{\mathrm{EV}}$ counterpart. In the mixed-integer case convexity is lost.

In risk averse optimization, the setting may be quite comfortable if a convexity preserving risk measure, such as the expected excess, is applied to a convex cost function. It is less comfortable for the excess probability which is not convexity preserving and, on finite probability spaces for instance, induces Boolean model variables for the calculation of discrete probabilities.

Finite dimensional counterparts to the stochastic cost functionals $\mathcal{Q}_{\mathrm{EV}}$, $\mathcal{Q}_{\mathrm{EE}_\eta}$, and $\mathcal{Q}_{\mathrm{EP}_\eta}$ thus are not always well suited to descent methods. While the linear case may benefit from the mentioned convexity, although nonsmoothness remains, the practically much more relevant mixed-integer linear case is inherently nonconvex, yet discontinuous.

Algorithmic treatment in finite dimension is mainly inspired by block structured large-scale equivalent model reformulations as linear or mixed-integer linear programs. These models become tractable by combining decomposition approaches with advanced mixed-integer linear programming methodology. Decomposition is driven by convex duality. The mixed-integer techniques rely on implicit enumeration (branch-and-bound), essentially avoiding complete enumeration. These alternatives, in contrast to pure descent methods, allow for the computation of provably globally optimal solutions.

In the infinite dimensional setting of the present paper, various complicating features are becoming algorithmically relevant. When formulating large-scale equivalents for minimizing (8), there are no obvious departure points for decomposition in analogy to finite dimension: The shape space lacks linear structure, such that the usual convexity and derived duality lack foundation. With Boolean variables, as for the excess probability for instance, one ends up with mixed-integer PDE constrained optimization. It is completely open how to handle this for the problem class at hand without resorting to complete enumeration.

These deficiencies leave a descent approach as conceptual alternative, with shortcomings of course. The empirical observation that already $J(x,\omega)$ may oscillate heavily endangers the iteration to get stuck at local optima. Cut-off effects by the excess probability or the expected excess create "flat regions" of the objective where the descent tends to come to a standstill, although there could be progress "nearby". The smooth approximation of the excess probability functional only seemingly removes the combinatorial complexity. If the approximation is very precise, then the mentioned standstill is more likely, leading to re-starts and de facto complete enumeration. If the approximation is less precise, then the tendency to descend from plateaus is promoted, but the approximate might have too little to do with the original objective. In our computations we aimed at striking a proper compromise here.

Summing up, a descent approach, as taken in this paper, clearly would be inferior in finite dimension. In infinite dimension, to our best knowledge, it so far is the only numerically viable alternative.

Acknowledgment

References

[1] ADALI, S., J.C. BRUCH, J., SADEK, I., AND SLOSS, J. Robust shape control of beams with load uncertainties by optimally placed piezo actuators. *Structural and Multidisciplinary Optimization 19*, 4 (2000), 274–281.

[2] ALLAIRE, G. *Shape Optimization by the Homogenization Method*, vol. 146. Springer Applied Mathematical Sciences, 2002.

[3] ALLAIRE, G. Topology optimization with the homogenization and the level-set methods. In *Nonlinear homogenization and its applications to composites, polycrystals and smart materials*, vol. 170 of *NATO Sci. Ser. II Math. Phys. Chem.* Kluwer Acad. Publ., Dordrecht, 2004, pp. 1–13.

[4] ALLAIRE, G., DE GOURNAY, F., JOUVE, F., AND TOADER, A.-M. Structural optimization using topological and shape sensitivity via a level set method. *Control and Cybernetics 34* (2005), 59–80.

[5] ALLAIRE, G., AND JOUVE, F. A level-set method for vibration and multiple loads structural optimization. *Comput. Methods Appl. Mech. Engrg. 194*, 30-33 (2005), 3269–3290.

[6] ALLAIRE, G., JOUVE, F., AND DE GOURNAY, F. Shape and topology optimization of the robust compliance via the level set method. *ESAIM Control Optim. Calc. Var. 14* (2008), 43–70.

[7] ALLAIRE, G., JOUVE, F., AND TOADER, A.-M. Structural optimization using sensitivity analysis and a level-set method. *Journal of Computational Physics 194*, 1 (2004), 363–393.

[8] ALVAREZ, F., AND CARRASCO, M. Minimization of the expected compliance as an alternative approach to multiload truss optimization. *Struct. Multidiscip. Optim. 29* (2005), 470–476.

[9] AMSTUTZ, S., AND ANDRÄ, H. A new algorithm for topology optimization using a level-set method. *Journal of Computational Physics 216* (2006), 573–588.

[10] BANICHUK, N. V., AND NEITTAANMÄKI, P. On structural optimization with incomplete information. *Mechanics Based Design of Structures and Machines 35* (2007), 75–95.

[11] BEN-TAL, A., KOČVARA, M., NEMIROVSKI, A., AND ZOWE, J. Free material design via semidefinite programming: the multiload case with contact conditions. *SIAM J. Optim. 9* (1999), 813–832.

[12] BEN-TAL, A., AND NEMIROVSKI, A. Robust optimization methodology and applications. *Mathematical Programming, Ser. B 92*, 3 (2002), 453–480.

[13] BENDSØE, M. P. *Optimization of structural topology, shape, and material.* Springer-Verlag, Berlin, 1995.

[14] BURGER, M., HACKL, B., AND RING, W. Incorporating topological derivatives into level set methods. *J. Comp. Phys. 194* (2004), 344–362.

[15] CHERKAEV, A., AND CHERKAEV, E. Stable optimal design for uncertain loading conditions. In *Homogenization*, V. B. et al., Ed., vol. 50 of *Series on Advances in Mathematics for Applied Sciences.* World Scientific, Singapore, 1999, pp. 193–213.

[16] CHERKAEV, A., AND CHERKAEV, E. Principal compliance and robust optimal design. *Journal of Elasticity 72* (2003), 71–98.

[17] CONTI, S., HELD, H., PACH, M., RUMPF, M., AND SCHULTZ, R. Shape optimization under uncertainty – a stochastic programming perspective. *SIAM J. Optim. 19* (2009), 1610–1632.

[18] DE GOURNAY, F., ALLAIRE, G., AND JOUVE, F. Shape and topology optimization of the robust compliance via the level set method. *ESAIM: Control, Optimisation and Calculus of Variations 14* (2007), 43–70.

[19] DELFOUR, M. C., AND ZOLÉSIO, J. *Geometries and Shapes: Analysis, Differential Calculus and Optimization.* Adv. Des. Control 4. SIAM, Philadelphia, 2001.

[20] DU, Q., AND WANG, D. Tetrahedral mesh generation and optimization based on centroidal Voronoi tesselations. *International Journal for Numerical Methods in Engineering 56* (2003), 1355–1373.

[21] EICHHORN, A., AND RÖMISCH, W. Polyhedral risk measures in stochastic programming. *SIAM J. on Optimization 16*, 1 (2005), 69–95.

[22] GARREAU, S., GUILLAUME, P., AND MASMOUDI, M. The topological asymptotic for PDE systems: The elasticity case. *SIAM J. Control Optim. 39*, 6 (2001), 1756–1778.

[23] GUEDES, J. M., RODRIGUES, H. C., AND BENDSØE, M. P. A material optimization model to approximate energy bounds for cellular materials under multiload conditions. *Struct. Multidiscip. Optim. 25* (2003), 446–452.

[24] HACKBUSCH, W., AND SAUTER, S. Composite finite elements for the approximation of PDEs on domains with complicated micro-structures. *Numerische Mathematik 75* (1997), 447–472.

[25] HE, L., KAO, C.-Y., AND OSHER, S. Incorporating topological derivatives into shape derivatives based level set methods. *Journal of Computational Physics 225*, 1 (2007), 891–909.

[26] HUYSE, L. *Free-form airfoil shape optimization under uncertainty using maximum expected value and second-order second-moment strategies.* ICASE report ; no. 2001-18. ICASE, NASA Langley Research Center Available from NASA Center for Aerospace Information, Hampton, VA, 2001.

[27] LIEHR, F., PREUSSER, T., RUMPF, M., SAUTER, S., AND SCHWEN, L. O. Composite finite elements for 3D image based computing. *Computing and Visualization in Science 12* (2009), 171–188.

[28] MELCHERS, R. Optimality-criteria-based probabilistic structural design. *Structural and Multidisciplinary Optimization 23*, 1 (2001), 34–39.

[29] OGRYCZAK, W., AND RUSZCZYŃSKI, A. Dual stochastic dominance and related mean-risk models. *SIAM J. on Optimization 13*, 1 (2002), 60–78.

[30] OSHER, S., AND FEDKIW, R. *Level set methods and dynamic implicit surfaces*, vol. 153 of *Applied Mathematical Sciences.* Springer-Verlag, New York, 2003.

[31] OSHER, S. J., AND SETHIAN, J. A. Fronts propagating with curvature dependent speed: algorithms based on hamilton-jacobi formulations. *Journal of Computational Physics 79* (1988), 12–49.

[32] OWEN, S. J. A survey of unstructured mesh generation technology. In *Proceedings of the 7th International Meshing Roundtable* (Dearborn, Michigan, 1998), Sandia National Laboratories, pp. 239–267.

[33] PFLUG, G. CH.; RÖMISCH, W. *Modeling, Measuring and Managing Risk*. World Scientific, Singapore, 2007.

[34] RIIS, M., AND SCHULTZ, R. Applying the minimum risk criterion in stochastic recourse programs. *Comput. Optim. Appl. 24*, 2-3 (2003), 267–287.

[35] ROCKAFELLAR, R. T., URYASEV, S., AND ZABARANKIN, M. Generalized deviations in risk analysis. *Finance and Stochastics 10*, 1 (01 2006), 51–74.

[36] RUMIGNY, N., PAPADOPOULOS, P., AND POLAK, E. On the use of consistent approximations in boundary element-based shape optimization in the presence of uncertainty. *Comput. Methods Appl. Mech. Engrg. 196* (2007), 3999–4010.

[37] RUSZCZYŃSKI, A., AND SHAPIRO, A., Eds. *Handbooks in Operations Research and Management Sciences, 10: Stochastic Programming*. Elsevier, Amsterdam, 2003.

[38] RUSZCZYŃSKI, A., AND SHAPIRO, A. Optimization of convex risk functions. *Math. Oper. Res. 31*, 3 (2006), 433–452.

[39] SCHULTZ, R., AND TIEDEMANN, S. Risk aversion via excess probabilities in stochastic programs with mixed-integer recourse. *SIAM J. on Optimization 14*, 1 (2003), 115–138.

[40] SCHULTZ, R., AND TIEDEMANN, S. Conditional value-at-risk in stochastic programs with mixed-integer recourse. *Math. Program. 105*, 2-3 (2006), 365–386.

[41] SCHUMACHER, A. *Topologieoptimierung von Bauteilstrukturen unter Verwendung von Lochpositionierungskriterien*. PhD thesis, Universitat – Gesamthochschule Siegen, 1996.

[42] SOKOŁOWSKI, J., AND ŻOCHOWSKI, A. On the topological derivative in shape optimization. *SIAM J. Control Optim. 37*, 4 (1999), 1251–1272.

[43] SOKOŁOWSKI, J., AND ŻOCHOWSKI, A. Topological derivatives of shape functionals for elasticity systems. *Mech. Struct. & Mach. 29*, 3 (2001), 331–349.

[44] SOKOŁOWSKI, J., AND ŻOCHOWSKI, A. Optimality conditions for simultaneous topology and shape optimization. *SIAM Journal on Control and Optimization 42*, 4 (2003), 1198–1221.

[45] SOKOŁOWSKI, J., AND ZOLÉSIO, J.-P. *Introduction to Shape Optimization: Shape Sensitivity Analysis*. Springer, 1992.

[46] ZHUANG, C., XIONG, Z., AND DING, H. A level set method for topology optimization of heat conduction problem under multiple load cases. *Comput. Methods Appl. Mech. Engrg. 196* (2007), 1074–1084.